A Coherent Single-Hole Spin in a Semiconductor

Daniel Brunner, *et al.*
Science **325**, 70 (2009);
DOI: 10.1126/science.1173684

turbulence and convection, so that in the early evening, the mixing ratio of water vapor was approximately constant up to a height of 4 km. Above the cloud top, the water vapor partial pressure would have been below the saturation value because clouds were not observed at those heights. The corresponding height profile of frost point temperature (before cloud formation) is shown in Fig. 1C. The integrated amount of water vapor within the PBL (from the ground to 4 km) before cloud formation on sol 99 ($L_s = 122°$) can be estimated from the analysis above to be 35 pr-μm. This is a substantial fraction of the total atmospheric column water vapor (40 to 50 pr-μm) measured from orbit at the latitude of Phoenix in previous years (1, 16). Solar radiation measurements during the Pathfinder mission also indicated that atmospheric water vapor was confined near the ground (17).

We also used the simulated temperature profiles in Fig. 1C to estimate the IWC in the clouds. At 05:00 and a height of 4 km, the simulated temperature is –66°C and the saturated vapor density is 5 mg m^{-3}. The threshold value of vapor density at cloud formation (time 01:00) was 7.6 mg m^{-3}. The difference of 2.6 mg m^{-3} is an estimate of the IWC in the cloud, and this is within the range of IWC derived from the LIDAR measurements.

Our estimate of the water content of the PBL is consistent with independent measurements. The Thermal and Electrical Conductivity Probe instrument (18) on Phoenix measured the partial pressure of water vapor near the ground to have values up to 2 Pa during the daytime and less than 0.1 Pa at night, with a diurnal average of 0.9 Pa (6). The water vapor volume mixing ratio in the mixed boundary layer would be greater than the average at ground level (0.0012), because the

vertical mixing occurs mainly during the daytime. Also, if the water vapor volume mixing ratio was 0.0016 throughout the PBL, then the integrated amount up to a height of 4 km would be 40 pr-μm, and this is an upper limit because it is within the measured range of the total atmospheric column water vapor (1, 16). Our estimate of the volume mixing ratio at the top of the PBL (0.0014) is within the range of plausible values.

The Phoenix LIDAR observations have demonstrated that water-ice crystals grow large enough to precipitate through the atmosphere of Mars. In the early morning hours, the clouds formed at ground level and at heights around 4 km because these were the coldest parts of the PBL (Fig. 1C). The cloud was capped at the top of the PBL because daytime turbulent mixing does not transport moisture above that height. The overall process was that water ice was transported downward by precipitation at night, it sublimated in the morning, and then the vapor was mixed back up through the PBL by turbulence and convection during the daytime. The clouds and precipitation act to confine water within the PBL. Eventually the ice clouds would have persisted within the PBL throughout the daytime, and water ice would have remained deposited on the ground. As the depth of the PBL decreased in late summer, this local process would contribute to the seasonal decrease in atmospheric water vapor (1).

References and Notes

1. M. D. Smith et al., J. Geophys. Res. **107**, 5115 10.1029/2001JE001522 (2002).
2. D. Davies, J. Geophys. Res. **84**, 8335 (1979).
3. J. Ryan et al., J. Geophys. Res. **87**, 7279 (1982).
4. R. A. Kahn, J. Geophys. Res. **95**, 14677 (1990).
5. P. H. Smith et al., J. Geophys. Res. **113**, E00A18 (2008).
6. P. H. Smith et al., Science **325**, 58 (2009).
7. J. A. Whiteway et al., J. Geophys. Res. **113**, E00A08 10.1029/2007JE003002 (2008).
8. A sol is a martian day, with a length of 24.6 hours. Phoenix landed 30 sols before the Mars summer solstice, when solar longitude is $L_s = 90°$.
9. Materials and methods are available as supporting material on Science Online.
10. Further evidence of precipitation was observed in images of low-level clouds (supporting online material text).
11. N. A. Fuchs, The Mechanics of Aerosols (Pergamon, New York, 1964).
12. J. A. Whiteway et al., Geophys. Res. Lett. **31**, L24102 (2004).
13. M. W. Gallagher et al., Q. J. R. Meteorol. Soc. **131**, 1143 (2005).
14. A. J. Heymsfield et al., Geophys. Res. Lett. **32**, L10807 (2005).
15. P. R. Field et al., Atmos. Chem. Phys. **6**, 2991 (2006).
16. H. Tschimmel et al., Icarus **195**, 557 (2008).
17. D. V. Titov et al., J. Geophys. Res. **104**, 9019 (1999).
18. A. P. Zent et al., J. Geophys. Res. **114**, E00A27 (2009).
19. R. Davy et al., J. Geophys. Res. **114**, D04108 (2009).
20. For the simulations used here, the upper-level wind was assumed to be as 5 m s^{-1}. The temperature and pressure at ground level were matched to the Phoenix in situ measurements, and the height distribution of dust was based on the Phoenix LIDAR observations. The model predicts a PBL depth of 4 km, which is consistent with the LIDAR daytime dust observations (Fig. 1A).
21. We acknowledge contributions to landed operations from the engineering staff at the CSA (P. Allard, C. Brunet, D. Cormier, I. Tremblay, and E. Vachon) and MDA Space Missions (D. Hill, L. Clark, A. Kerr, and R. McCoubrey). This work was enabled by funding from the CSA under contract 9F007-070437/001/SR. The Phoenix mission was led by the University of Arizona, on behalf of NASA, and managed by the Jet Propulsion Laboratory.

A Coherent Single-Hole Spin in a Semiconductor

Daniel Brunner,[1] Brian D. Gerardot,[1] Paul A. Dalgarno,[1] Gunter Wüst,[1] Khaled Karrai,[2] Nick G. Stoltz,[3] Pierre M. Petroff,[3] Richard J. Warburton[1,4]*

Semiconductors have uniquely attractive properties for electronics and photonics. However, it has been difficult to find a highly coherent quantum state in a semiconductor for applications in quantum sensing and quantum information processing. We report coherent population trapping, an optical quantum interference effect, on a single hole. The results demonstrate that a hole spin in a quantum dot is highly coherent.

Semiconductor heterostructures can be designed to confine electrons, holes, and photons in specific ways. Post-growth processing enables the creation of individual devices and their interconnection into fully functional circuits. However, it is not yet clear whether these material advantages can be exploited in a new class of device whose operation depends on the controlled manipulation of coherent quantum states. Achieving the necessary coherence poses considerable challenges.
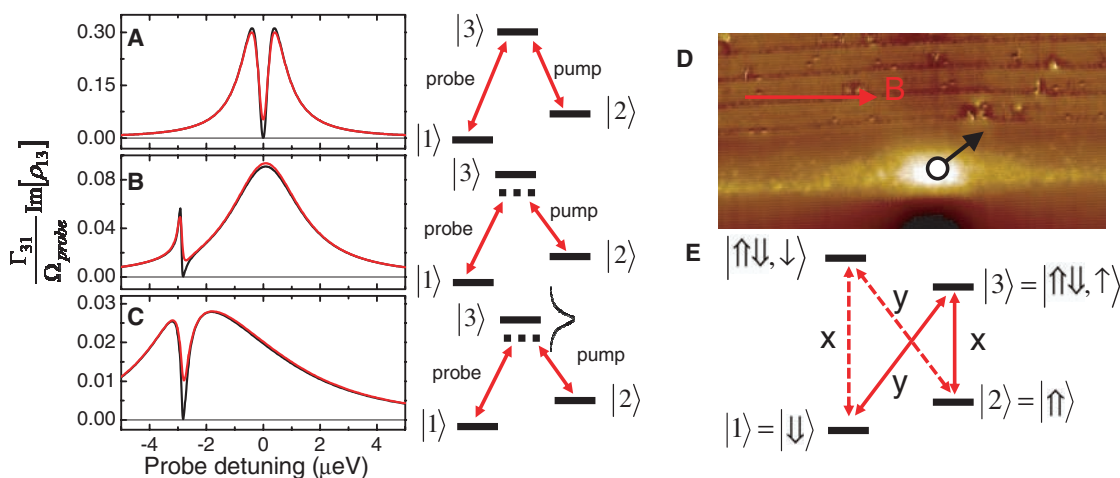
In bulk semiconductors and quantum wells, individual quantum states lose coherence rapidly through an interaction with the lattice vibrations, or phonons. An electron spin interacts only indirectly via the spin-orbit interaction with the phonons and emerges as a strong candidate quantum bit (qubit) (1). However, to suppress the spin-orbit interaction, the electron must be tightly confined to a nanoscopic quantum dot (2–4). But in GaAs, the semiconductor with the best materials properties, the electron spin now interacts with 10^4 to 10^5 nuclear spins, too few for cancellation of the hyperfine interaction and too many for each nuclear spin to be used as a resource. The nuclear spins create a fluctuating effective magnetic field, the Overhauser field. The electron spin precesses in the Overhauser field such that the time-averaged coherence time, T_2^*, is small, just ~10 ns (5–7), much less than the intrinsic decoherence time, T_2, which is around 1 μs (8, 9). This difficulty represents a stumbling block in engineering a coherent semiconductor spin state.

[1]School of Engineering and Physical Sciences, Heriot-Watt University, Edinburgh EH14 4AS, UK. [2]Department für Physik der Ludwig-Maximilians-Universität, Geschwister-Scholl-Platz 1, 80539 Munich, Germany. [3]Materials Department, University of California, Santa Barbara, CA 93106, USA. [4]Department of Physics, University of Basel, Klingelbergstrasse 82, 4056 Basel, Switzerland.

*To whom correspondence should be addressed. E-mail: r.j.warburton@hw.ac.uk

Fig. 1. (**A**) Calculated probe absorption spectrum in the presence of an on-resonant pump laser in a Λ system. The dip represents CPT; ρ is the density matrix. (**B**) As for (A) but with a detuned pump. The model uses Rabi energies $\hbar\Omega_{pump} = 1.0$ μeV, $\hbar\Omega_{probe} = 0.45$ μeV, radiative decay rates $\hbar\Gamma_{31} = \hbar\Gamma_{32} = \frac{1}{2}\hbar\Gamma_r = 0.50$ μeV with a lower-level coherence time $T_2 = 1$ μs (black line), and $T_2 = 10$ ns (red line). (**C**) Calculated probe absorption with the same parameters as (B) but also including a spec-

tral wandering of level $|3\rangle$ with Lorentzian probability distribution with full width $\Gamma_\chi = 6$ μeV. (**D**) A cross-sectional scanning tunneling image (80 nm by 40 nm) of a quantum dot, showing schematically a single hole and a magnetic field B applied in the plane along the x direction. [Image: Murat Bozkurt and Paul Koenraad] (**E**) The quantum states of the hole: $|1\rangle$ and $|2\rangle$ are the hole spin eigenvectors in the x basis, split by the Zeeman effect; the upper levels are X^{1+} excitons consisting of two spin-paired holes and an unpaired electron with spin $\pm\frac{1}{2}$, again in the x basis. The optical transitions are linearly polarized along either the x or y direction. Two Λ systems are established (solid and dashed lines).

An alternative is to use a hole spin in an attempt to bypass the interaction with the nuclear spins (*10–16*). A hole state is constructed from a p-type atomic wave function that conveniently goes to zero at the location of the nuclei, suppressing the contact part of the hyperfine interaction (*14*). Furthermore, in a quantum dot, the hole spin–phonon interaction is weak because the strong quantization reduces the admixture of heavy and light hole states (*11, 13*).
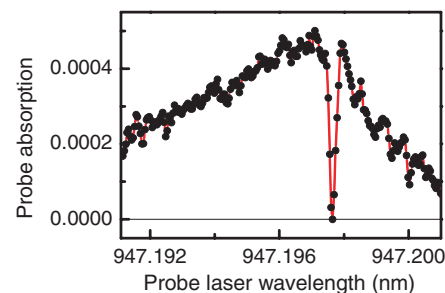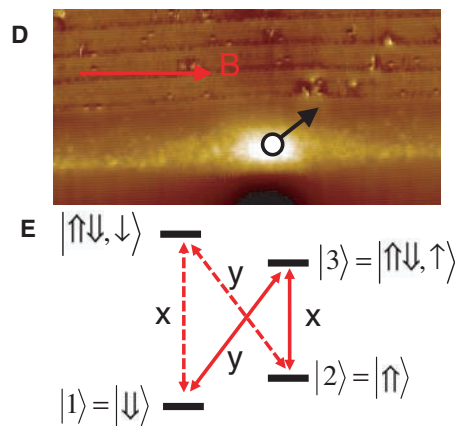
We conducted an experiment that is sensitive to hole spin coherence. We observed a quantum interference phenomenon, the "visibility" of which depends directly on the hole spin coherence (*17*). The interference arises in the optical spectroscopy of a Λ system, a quantum system consisting of three states, $|1\rangle$, $|2\rangle$, and $|3\rangle$, with optical transitions between $|1\rangle \leftrightarrow |3\rangle$ and $|2\rangle \leftrightarrow |3\rangle$ (Fig. 1A). In our case, states $|1\rangle$ and $|2\rangle$ correspond to Zeeman-split hole spin states, and state $|3\rangle$ corresponds to an exciton. A "pump" laser [Rabi energy $\hbar\Omega_{pump}$, where $\hbar$ is Planck's constant divided by 2π] drives the $|2\rangle \leftrightarrow |3\rangle$ transition, and a "probe" laser [Rabi energy $\hbar\Omega_{probe}$] drives the $|1\rangle \leftrightarrow |3\rangle$ transition. The interference occurs when the frequency difference of the lasers matches the $|1\rangle$-$|2\rangle$ splitting, the two-photon resonance. In this case, the amplitude of state $|3\rangle$ undergoes a destructive interference, and a dark state—an admixture consisting only of states $|1\rangle$ and $|2\rangle$—results. This phenomenon, coherent population trapping (CPT) (*7, 17–20*), is the underlying basis for electromagnetically induced transparency (*21*) and is revealed by a dip in the probe absorption spectrum, provided that the coherence of states $|1\rangle$ and $|2\rangle$ is high enough. Specifically, when $\Gamma_r > \Omega_{pump} > \Omega_{probe}$, the probe absorption acquires a dip with energy width $\hbar\Omega^2_{pump}/\Gamma_r$ where Γ_r is the spontaneous emission rate from state $|3\rangle$ (Fig. 1A). This width sets the sensitivity of the experiment to the decoherence rate γ of state $|2\rangle$ with respect to $|1\rangle$: For $\gamma \ll \Omega^2_{pump}/\Gamma_r$ the signal in the dip goes to

zero, but for $\gamma \gg \Omega^2_{pump}/\Gamma_r$ the dip is washed out (Fig. 1A). Previous observations of CPT in semiconductors have not achieved a perfect dip because in each case the dephasing was too rapid (*7, 18–20*).

Our experiments are performed on single InGaAs dots in a GaAs matrix (Fig. 1D), loading a single hole into a single dot and probing the exciton transitions resonantly with laser spectroscopy (*22*). To establish a Λ system, we apply a magnetic field in the x direction, in the growth plane, which allows optical transitions from both hole spin states to both exciton states (*23*) (Fig. 1E). Once the Zeeman splitting of the exciton states is larger than the linewidths, two Λ systems can be established. We work with the one at lower energy (Fig. 1E). At zero magnetic field and with one linearly polarized laser, there is an absorption peak at the exciton resonance. In magnetic field, this resonance disappears through optical pumping (*4, 23*). However, a "double resonance" can be located by driving the dot simultaneously with a second laser: When both lasers come into resonance, one with the $|1\rangle \leftrightarrow |3\rangle$ transition and the other with the $|2\rangle \leftrightarrow |3\rangle$ transition, optical pumping is suppressed and a probe absorption signal reappears. Upon locating the double resonance, we then look for the CPT dip.

In the example data at a magnetic field of 2.3 T (Fig. 2), there is a pronounced and narrow dip in the probe spectrum. To prove that the dip arises from CPT, we detuned the pump laser (Fig. 3, A to C). Figure 3D shows that the energy shift of the dip in the probe spectrum equals the energy shift of the pump, as expected for a two-photon resonance. There are a number of features in Fig. 2. First, the dot is rendered transparent at the two-photon resonance. Such a clear destructive interference is only possible with a highly coherent hole spin state. Second, the CPT dip clearly survives the broadening of the exciton resonance, which is as large as 6 μeV for this particular dot.

Fig. 2. Measured probe absorption spectrum (differential reflectivity) in the presence of a close-to-resonant weak pump laser on a single quantum dot containing a single hole. The pronounced dip signifies CPT. The measured Rabi energies are $\hbar\Omega_{pump} = 0.75 \pm 0.25$ μeV and $\hbar\Omega_{probe} = 0.34 \pm 0.15$ μeV; radiative decay time, 0.4 ± 0.2 ns; magnetic field, 2.3 T; integration time per point, 5 s; temperature, 4.2 K.

Third, for nonzero pump detunings, the form of the probe absorption spectrum does not follow the atomic physics model (Fig. 1B). Instead of a maximum signal located close to zero probe detuning (Fig. 1B), we find that the maximum signal is always close to the CPT dip (Fig. 3, A and C). Furthermore, for positive pump detunings, the probe absorption falls more rapidly on the positive detuning side than on the negative side, a situation reversed for negative pump detunings.

The CPT dip allows us to make a quantitative statement on the hole spin coherence time T_2^* (*17*). To eliminate systematic errors, it is first necessary to understand the entire probe spectrum (Fig. 3, A to C). The missing factor in Fig. 1, A and B, is a description of the broadening of state $|3\rangle$, the exciton. Including subnanosecond dephasing in level $|3\rangle$ fails; this simply smears out the curves in Fig. 1, A and B. The experiment itself points to the resolution of this problem. The
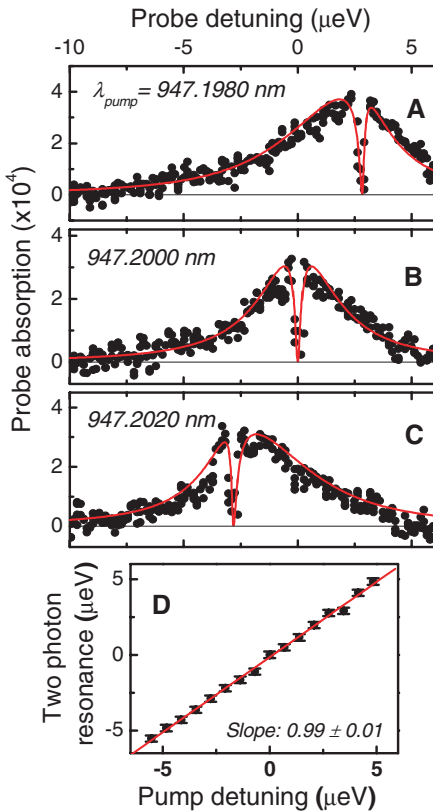
Fig. 3. CPT of a single-hole spin at 3.0 T and 4.2 K with Zeeman splitting 18.38 μeV using the same dot and Rabi energies as Fig. 2. The points show the measured absorption against probe laser detuning for three different pump wavelengths, one blue-detuned from the resonance (**A**), one close to resonance (**B**), and one red-detuned (**C**). The solid lines are fits to the calculated response for pump detunings of +2.831 μeV (A), 0.000 μeV (B), and −2.820 μeV (C); $\hbar\Omega_{pump} = 1.0$ μeV, $\hbar\Omega_{probe} = 0.45$ μeV, $\hbar\Gamma_{31} = \hbar\Gamma_{32} = 0.50$ μeV, $\hbar\gamma_3 = 0$ (pure dephasing rate of state $|3\rangle$), $\hbar\gamma_2 = 0.00067$ μeV, $\Gamma_x = 6.0$ μeV, and field scattering ratio $\alpha = 0.01$ (*22*). (**D**) Measured detuning of the probe laser at the CPT dip plotted against pump laser detuning with a linear fit.

narrow CPT dip amid the broad exciton resonance suggests that the exciton undergoes a spectral wandering with little if any effect on the hole spin splitting. Once the two-photon resonance condition is satisfied, it remains satisfied even as the exciton energy fluctuates. To confirm this view, we convoluted the density matrix calculation with a probability distribution in the detunings to describe the fluctuations of the exciton energy, slow relative to radiative recombination but fast relative to the experimental integration (*22*). The convolution made surprisingly large changes to the probe spectrum (Fig. 1C) and reproduced all the features in the experiment. We achieved excellent fits to the probe absorption curves (Fig. 3, A to C), reproducing both the width of the CPT dip and the overall line shape.
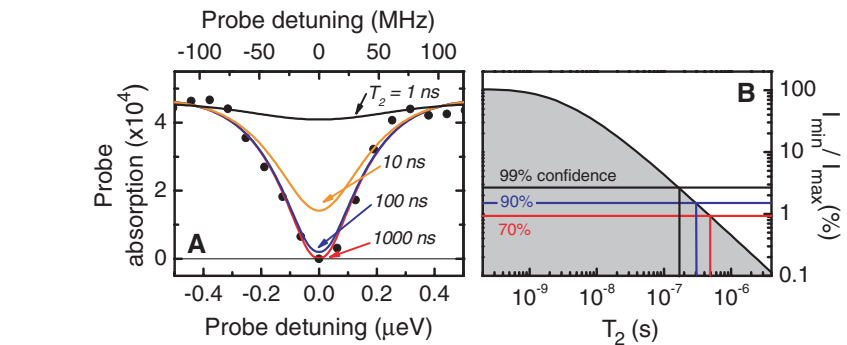
Fig. 4. (**A**) Data from Fig. 2 versus the calculated response (solid line) for several values of hole spin T_2. The theory uses the same parameters as in Fig. 3. (**B**) The calculated signal in the dip divided by the maximum signal (at zero pump detuning) as a function of hole spin T_2 (solid line). Experimental minimum/maximum signal ratios for confidence levels of 99%, 90%, and 70% are shown with horizontal lines.

The minimum signal in the dip depends on the hole spin coherence. Figure 4A shows the results of the theory for various T_2 values along with the data of Fig. 2, allowing an immediate and robust conclusion that T_2^* is at least 100 ns. To quantify this upper bound further, we used the average of the ratio of the minimum to the maximum signal, I_{min}/I_{max}, from 10 data sets: $(0.11 \pm 2.07)\%$. Figure 4B plots the calculated I_{min}/I_{max} versus T_2. The constraints on the parameters are that they must be compatible with the auxiliary experiments (*22*) and that they reproduce the overall line shapes in Fig. 3. This implies that any systematic error is less than the random error in the measurement of the small signal in the dip. The data in Fig. 4 reveal upper bounds to T_2 associated with probabilities calculated from the random error, for example, $T_2 \geq 490$ ns with 70% probability. With the current data, the probability that T_2 exceeds 1 μs is about 40%.

The CPT dip (Fig. 2 and Fig. 3, A to C) has a linewidth of just 0.35 μeV (85 MHz), ushering semiconductor optical spectroscopy into the domain of atomic physics with applications as frequency standards (*24*), ultrasensitive magnetometers (*25*), "slow light" photon storage devices (*21*), and coherent spin rotations via stimulated Raman adiabatic passage (*26*). The coherence of the hole spin points to applications in quantum information. A two-qubit device is possible with hole spins in tunnel-coupled quantum dot molecules (*27*).

The contact hyperfine interaction is not the only interaction between a quantum dot spin and the nuclear spins. There is also a dipole-dipole interaction. Recent theory suggests that the coupling coefficient of the heavy hole dipole-dipole hyperfine interaction is by no means negligible (*28*), but the interaction has an Ising form. For electrons, loss of phase arises through the component of the Overhauser field along the direction of the applied field. For a heavy hole spin with an Ising interaction, the Overhauser field lies in the growth direction, z, and has a benign effect in the presence of a large applied field in the x direction. Our data are consistent with this picture, but further work is required to establish its validity.

References and Notes

1. R. Hanson, L. P. Kouwenhoven, J. R. Petta, S. Tarucha, L. M. K. Vandersypen, *Rev. Mod. Phys.* **79**, 1217 (2007).
2. M. Kroutvar *et al.*, *Nature* **432**, 81 (2004).
3. S. Amasha *et al.*, *Phys. Rev. Lett.* **100**, 046803 (2008).
4. J. Dreiser *et al.*, *Phys. Rev. B* **77**, 075317 (2008).
5. I. A. Merkulov, A. L. Efros, M. Rosen, *Phys. Rev. B* **65**, 205309 (2002).
6. M. H. Mikkelsen, J. Berezovsky, N. G. Stoltz, L. A. Coldren, D. D. Awschalom, *Nat. Phys.* **3**, 770 (2007).
7. X. Xu *et al.*, *Nat. Phys.* **4**, 692 (2008).
8. J. R. Petta *et al.*, *Science* **309**, 2180 (2005); published online 1 September 2005 (10.1126/science.1116955).
9. A. Greilich *et al.*, *Science* **313**, 341 (2006).
10. S. Laurent *et al.*, *Phys. Rev. Lett.* **94**, 147401 (2005).
11. D. V. Bulaev, D. Loss, *Phys. Rev. Lett.* **95**, 076805 (2005).
12. M. Syperek *et al.*, *Phys. Rev. Lett.* **99**, 187401 (2007).
13. D. Heiss *et al.*, *Phys. Rev. B* **76**, 241306 (2007).
14. B. D. Gerardot *et al.*, *Nature* **451**, 441 (2008).
15. A. J. Ramsay *et al.*, *Phys. Rev. Lett.* **100**, 197401 (2008).
16. B. Eble *et al.*, *Phys. Rev. Lett.* **102**, 146601 (2009).
17. A. Imamoglu, *Phys. Stat. Sol. B* **243**, 3725 (2006).
18. M. D. Frogley, J. F. Dynes, M. Beck, J. Faist, C. C. Phillips, *Nat. Mater.* **5**, 175 (2006).
19. K. M. C. Fu, C. Santori, C. Stanley, M. C. Holland, Y. Yamamoto, *Phys. Rev. Lett.* **95**, 187405 (2005).
20. M. C. Phillips *et al.*, *Phys. Rev. Lett.* **91**, 183602 (2003).
21. M. Fleischhauer, A. Imamoglu, J. P. Marangos, *Rev. Mod. Phys.* **77**, 633 (2005).
22. See supporting material on *Science* Online.
23. X. Xu *et al.*, *Phys. Rev. Lett.* **99**, 097401 (2007).
24. R. Wynands, A. Nagel, *Appl. Phys. B* **68**, 1 (1999).
25. M. O. Scully, M. Fleischhauer, *Phys. Rev. Lett.* **69**, 1360 (1992).
26. K. Bergmann, H. Theuer, B. W. Shore, *Rev. Mod. Phys.* **70**, 1003 (1998).
27. E. A. Stinaff *et al.*, *Science* **311**, 636 (2006); published online 11 January 2006 (10.1126/science.1121189).
28. J. Fischer, W. A. Coish, D. V. Bulaev, D. Loss, *Phys. Rev. B* **78**, 155329 (2008).
29. Supported by the UK Engineering and Physical Sciences Research Council and the Royal Society of Edinburgh.